NASA TN D-129

TECHNICAL NOTE
D-129

COMBINED EFFECT OF CONTRACTION RATIO AND CHAMBER PRESSURE ON THE PERFORMANCE OF A GASEOUS-HYDROGEN - LIQUID-OXYGEN COMBUSTOR FOR A GIVEN PROPELLANT WEIGHT FLOW AND OXIDANT-FUEL RATIO

By Martin Hersch

Lewis Research Center
Cleveland, Ohio

NATIONAL AERONAUTICS AND SPACE ADMINISTRATION
WASHINGTON

February 1961

NATIONAL AERONAUTICS AND SPACE ADMINISTRATION

TECHNICAL NOTE D-129

COMBINED EFFECT OF CONTRACTION RATIO AND CHAMBER PRESSURE ON THE PERFORMANCE OF A GASEOUS-HYDROGEN - LIQUID-OXYGEN COMBUSTOR FOR A GIVEN PROPELLANT WEIGHT FLOW AND OXIDANT-FUEL RATIO

By Martin Hersch

SUMMARY

The effect of contraction ratio and chamber pressure on the combustion performance of a gaseous-hydrogen - liquid-oxygen combustor was investigated analytically and experimentally. The experiment was conducted with a "two-dimensional" gaseous-hydrogen - liquid-oxygen engine of about 150-pound thrust. The contraction ratio was varied from 1.5 to 6 by changing the nozzle throat area. This variation resulted in a chamber pressure variation of about 25 to 120 pounds per square inch. The experimental results were corrected for heat transfer to the engine walls and momentum pressure losses.

The experimental performance, as evaluated in terms of characteristic exhaust velocity, was 98 percent of theoretical at contraction ratios greater than 3 but decreased very rapidly at smaller contraction ratios. The heat-transfer rate increased with increasing contraction ratio and chamber pressure; it was about 1 Btu per square inch per second at a contraction ratio of 1.5 and increased to about 3 at a contraction ratio of 6.

The combined effects of contraction-ratio and chamber-pressure changes on performance were investigated analytically with a mixing model and a vaporization model. The mixing model predicted very poor mixing at contraction ratios below 3 and almost perfect mixing at higher contraction ratios. The performance predicted by the vaporization model was very close to 100 percent for all contraction ratios.

From these results, it was concluded that the performance was limited by poor mixing at low contraction ratios and chamber pressures.

INTRODUCTION

Recent developments in rocket technology have indicated that low-chamber-pressure and low-contraction-ratio engines may be advantageous in certain applications. This is provided, however, that there is not a serious performance penalty at the lower pressures and contraction ratios.

The purpose of this paper is to determine the combustion losses, if any, at low contraction ratios and chamber pressures and to explain these losses analytically. The chamber-pressure and contraction-ratio changes in this study were produced by varying the nozzle throat area. All other operating conditions were held approximately constant. Characteristic exhaust velocity c^* was determined with a gaseous-hydrogen - liquid-oxygen combustor of about 150-pound thrust at a total propellant flow rate of 0.610 pound per second and an oxidant-fuel ratio of 3.2, corresponding to peak theoretical characteristic exhaust velocity.

APPARATUS AND PROCEDURE

Combustor

The engine, shown diagrammatically in figure 1, approximated a "two-dimensional" configuration, having a 1- by 8-inch rectangular cross section for combustion. The total engine length was $13\frac{7}{8}$ inches, including 3 inches of nozzle; the engine walls were 1 inch thick.

The chamber pressure was varied from 25 to 120 pounds per square inch by means of a set of interchangeable nozzle blocks bolted onto the engine. The throat areas and corresponding contraction ratios are as follows:

Contraction ratio	Nozzle throat area, sq in.
1.5	5.33
2	4.00
3	2.67
4	2.00
5	1.60
6	1.33

The nozzle cross sections were also rectangular, with the chamber width of 1 inch preserved to the nozzle exit. The chamber and the nozzle blocks were made of uncooled copper.

Injector

A concentric tube-type injector was used, three elements of which are shown in figure 2. There were 30 such elements arranged in a straight line parallel to the long dimension of the injector along the centerline, with 1/4-inch hole spacing. The oxygen tubes had an inner diameter of 0.047 inch and were about $1\frac{7}{8}$ inches long; they were concentric with gaseous hydrogen orifices of 0.1285-inch diameter and 1/4-inch length.

Test Facilities

A pressurized-tank propellant flow system was used. Liquid-oxygen temperature was stabilized by submergence of the oxygen flow system in a boiling liquid-nitrogen bath.

Performance Measurements

Engine performance was evaluated in terms of characteristic exhaust velocity c*, which was calculated from measurements of chamber pressure, propellant weight flow, and nozzle throat area.

Chamber pressure was measured by both a Bourdon tube and a strain-gage-type transducer, both sharing a common pressure measurement tap in the engine wall $1\frac{1}{2}$ inches downstream of the injector, as shown in figure 1.

Liquid-oxygen flow was measured with a rotating-vane-type flowmeter. The output of this meter was recorded directly as frequency and also as a direct-current voltage.

Gaseous-hydrogen flow was measured with a standard ASME orifice. The flow was computed from measurements of pressure and temperature above the meter and the pressure drop across the orifice.

The maximum possible random error in c* values measured with this instrumentation was approximately $\pm 2\frac{1}{2}$ percent.

Procedure

Five or more runs of 2.2-second duration at each contraction ratio were used to evaluate the c* performance. Only those runs whose oxidant and fuel flow rates were within ±10 percent of the predetermined

values of 0.464 and 0.145 pound per second, respectively, were used. This gave a mean oxidant-fuel ratio of 3.2. In addition, any runs having irregular liquid-oxygen flow, as indicated by the direct-current voltage records of oxidant flow, were discarded. The performance data are shown in table I.

Correction of Observed Performance

The observed c^* values were corrected for heat-transfer losses and momentum-pressure losses. The value of the theoretical c^* was also corrected for the enthalpy change in the propellants due to the use of gaseous rather than liquid hydrogen. The heat-transfer loss and enthalpy corrections were made by the method presented in reference 1, which treats the heat losses of the combustion gases to the engine walls and the enthalpy change in the propellants as a change in heat content of the combustion gases in the combustion chamber. The change in theoretical equilibrium c^* was from 8000 to 8240 feet per second at an oxidant-fuel ratio of 3.2. The heat-loss correction factors are listed in table II.

The momentum-pressure-loss correction is needed because the observed pressure was higher than the actual total pressure of the gases at the nozzle throat. The correction factors were computed with equations (3-13) and (3-41) of reference 2 and are given for each contraction ratio in table II.

Heat-Transfer Measurements

Although the engine was uncooled, an average overall heat-transfer rate was measured by using the engine structure as a calorimeter. The heat-transfer rate was thus calculated from the engine weight and specific heat, run-duration time, and temperature increase. The temperature increase was taken to be the difference between the initial engine temperature at the start of the run and the highest engine temperature reached after the end of the run. Both the fuel and oxidant flows were stopped simultaneously because the flow of cold propellant after shutdown would have affected the heat-transfer measurements. The total heat-absorption rate and per-unit area rate are given in table II. The engine temperature was detected with a thermocouple imbedded about 1/2 inch deep in one face about 5 inches below the injector, as shown in figure 1. A single thermocouple was sufficient because the high conductivity of the copper allowed the entire engine to approach a uniform temperature quickly after shutdown. Also, the heat losses of the engine to the surroundings were negligible, as evidenced by the long time needed for the engine to cool off after its maximum temperature was attained.

RESULTS AND DISCUSSION

The experimental characteristic-exhaust-velocity data are presented in table I; and the averaged c* values and efficiencies and the corrected efficiencies are presented in table II.

These corrected and averaged experimental results are shown in figure 3 as data points within a band whose width is that of the experimental error. The experimental performance appears to consist of two regions. One is a high-performance (98-percent) region above a contraction ratio of 3 and a pressure of 60 pounds per square inch; in this region, contraction-ratio changes have little effect on performance. The other region is below a contraction ratio of 3 and below chamber pressures of 60 pounds per square inch; in this region, the performance decreased very rapidly with decreasing contraction ratio and chamber pressure.

The effects of contraction ratio and combustion pressure on performance were also studied analytically by using both a mixing-limited and a vaporization-limited approach. The mixing model of reference 3 was used to determine mixing efficiency as a function of contraction ratio. The mixing efficiency, called a "ripple factor" in reference 3, is a measure of concentration variations at any given chamber length and has a value of unity for perfectly mixed gases. Mixing efficiencies at a chamber length of 10 inches were calculated for each contraction ratio. To calculate a mixing efficiency, the turbulence intensity (ratio of fluctuating to mean-stream velocity) was determined as follows: An experimental value of fluctuating velocity was obtained for a contraction ratio of 6 from reference 4. These measurements were made with the same engine used in the present study. The mean-stream velocity as a function of contraction ratio was calculated from equation (2) of reference 5. Then, with the assumption that the fluctuating velocity is independent of mean-stream velocity, as indicated in reference 4, the turbulence intensities were calculated by taking the ratio of fluctuating to mean-stream velocities. Mixing efficiencies were then determined from figure (6) of reference 3. The mixing efficiencies thus calculated are shown in figure 3 as a function of contraction ratio. This curve shows almost perfect mixing at contraction ratios greater than 3 but rapid falling off as the contraction ratio is decreased below 3.

The striking similarity of the experimental performance curve and the mixing efficiency curve of figure 3 suggests that the performance was mixing-limited at contraction ratios less than 3. This analysis would seem to indicate that performance, when limited by poor gas-phase mixing caused by low turbulence conditions, may perhaps be improved by increasing the ratio of chamber length to injector hole spacing.

The performance efficiency as a function of contraction ratio was also predicted with the vaporization model of reference 6. The vaporization-limited performance, however, was found to be very nearly 100 percent over the entire experimental range of pressures and contraction ratios. Therefore, it is unlikely that the loss in performance at low contraction ratios or chamber pressures was due to incomplete vaporization.

Poor performance at the lower contraction ratios may also have been due to low stay times of the gases at these contraction ratios. At a contraction of 1.5 the stay time is only about one-third that at a contraction ratio of 6. Therefore, the propellants had less time to mix and burn as the contraction ratio was decreased. However, in view of the very high chemical space heating rates, and therefore short reaction times as indicated in reference 7, it is doubtful whether the performance at the low chamber pressures and contraction ratios was chemically limited by reaction rates.

Limitations and Errors

One possible source of experimental error may have been boundary-layer buildup at the square corners of the nozzle. This would cause the effective throat area to be slightly smaller than that used in computing c* values and contraction ratios. The use of the effective throat area would have the effect of shifting the experimental curve of figure 3 slightly downward and to the right. This, however, would leave the performance trends unchanged.

Although the mixing model appears to offer a reasonable explanation for the experimental performance trend, it must be remembered, however, that the mixing calculations are at best only very approximate. The errors in the mixing calculations would be due to assumptions made regarding chamber gas velocity calculations, the value of the fluctuating velocity obtained from reference 4, and the extrapolation of the cold-flow conditions of reference 3 to combustion conditions. The values of intensity of turbulence used, however, are thought to be on the high side, which would tend to minimize the performance limitation indicated by the mixing model.

It must also be remembered that the mixing efficiency cannot be converted directly to c* values but should indicate performance trends. Although at off-stoichiometric propellant ratios complete mixing is unnecessary for complete combustion, high performance probably cannot be attained with poorly mixed gases.

SUMMARY OF RESULTS

The effects of chamber pressure and contraction ratio on combustor performance were investigated for a gaseous-hydrogen - liquid-oxygen combustor. The contraction ratio was varied from 1.5 to 6 with a resultant chamber pressure variation of about 25 to 120 pounds per square inch.

Experimentally the performance was very high, approximately 98 percent, at contraction ratios above 3 and chamber pressures greater than 60 pounds per square inch. As the contraction ratio and chamber pressure were decreased below these values, the performance decreased very rapidly. Analytically, it appeared that the poor performance in this region was caused by poor gas-phase mixing due to low turbulence conditions. This analysis indicated the possible importance of the ratio of chamber length to injector-hole spacing in combustors whose performance may be limited by gas-phase mixing. For such a combustor, a high value of this ratio may be needed in order to achieve a high performance.

Lewis Research Center
National Aeronautics and Space Administration
Cleveland, Ohio, November 23, 1960

E-1137

REFERENCES

1. Gordon, Sanford, and Huff, Vearl N.: Theoretical Performance of Liquid Hydrazine and Liquid Fluorine as a Rocket Propellant. NACA RM E53E12, 1953.

2. Sutton, George P.: Rocket Propulsion Elements. Second ed., John Wiley & Sons, Inc., 1956.

3. Bittker, David A.: An Analytical Study of Turbulent and Molecular Mixing in Rocket Combustion. NACA TN 4321, 1958.

4. Hersch, Martin: An Experimental Method of Measuring Intensity of Turbulence in a Rocket Chamber. Am. Rocket Soc. Jour., vol. 31, no. 1, Jan. 1961.

5. Heidmann, M. F., and Auble, C. M.: Injection Principles from Combustion Studies in a 200-Pound-Thrust Rocket Engine Using Liquid Oxygen and Heptane. NACA RM E55C22, 1955.

6. Priem, Richard J., and Heidmann, Marcus F.: Propellant Vaporization as a Design Criterion for Rocket-Engine Combustion Chambers. NASA TR R-67, 1960. (Supersedes NACA TN's 3883, 3985, 4098, and 4219.)

7. Bittker, David A., and Brokaw, Richard S.: Estimate of Chemical Space Heating Rates in Gas-Phase Combustion with Application to Rocket Propellants. Am. Rocket Soc. Jour., vol. 30, no. 2, Feb. 1960, pp. 179-185.

TABLE I. - EXPERIMENTAL DATA

Run	Fuel flow, lb/sec	Oxidant flow, lb/sec	Total flow, lb/sec	Oxidant-fuel ratio	Chamber pressure, lb/sq in. abs	Characteristic velocity, ft/sec
Contraction ratio, 1.5; nozzle area, 5.33 sq in.						
195	0.146	0.458	0.604	3.14	24.5	7080
196	.146	.456	.602	3.12	25.0	7240
197	.146	.461	.607	3.15	24.8	7110
199	.147	.466	.613	3.17	24.3	6910
207	.146	.481	.627	3.29	26.0	7230
Contraction ratio, 2.0; nozzle area, 4.00 sq in.						
213	0.141	0.478	0.619	3.39	33.0	7270
214	.151	.476	.627	3.15	33.0	7190
215	.148	.478	.626	3.23	33.9	7400
216	.148	.481	.629	3.25	34.2	7430
217	.147	.471	.618	3.20	32.9	7270
220	.148	.458	.606	3.10	32.7	7360
222	.146	.471	.617	3.22	32.7	7230
226	.149	.466	.615	3.13	34.2	7590
227	.150	.474	.624	3.16	32.2	7050
228	.150	.468	.618	3.12	33.2	7330
229	.150	.461	.611	3.07	33.5	7490
Contraction ratio, 3; nozzle area, 2.67 sq in.						
234	0.150	0.464	0.614	3.09	52.5	8040
235	.139	.466	.605	3.35	51.5	8000
236	.147	.468	.615	3.19	52.0	7940
237	.148	.474	.622	3.20	53.0	8010
238	.150	.476	.626	3.17	53.0	7950
239	.148	.481	.629	3.25	52.5	7840
242	.147	.493	.640	3.35	52.0	7640
243	.143	.466	.609	3.26	52.0	8030
246	.149	.477	.628	3.22	51.5	7710
247	.149	.479	.628	3.22	52.5	7860
249	.147	.488	.625	3.32	52.0	7830
250	.148	.466	.614	3.15	51.5	7890
251	.148	.471	.619	3.18	52.0	7900
Contraction ratio, 4; nozzle area, 2.00 sq in.						
183	0.138	0.471	0.609	3.41	67	7650
184	.144	.462	.606	3.21	67	7690
185	.141	.462	.603	3.27	66	7610
186	.142	.449	.591	3.16	67	7870
187	.144	.456	.600	3.17	67	7760
188	.143	.461	.604	3.22	67	7710
189	.143	.468	.611	3.28	68	7720
192	.143	.461	.604	3.22	67	7710
193	.144	.447	.591	3.10	67	7880
194	.144	.448	.592	3.11	65	7640

Run	Fuel flow, lb/sec	Oxidant flow, lb/sec	Total flow, lb/sec	Oxidant-fuel ratio	Chamber pressure, lb/sq in. abs	Characteristic velocity, ft/sec
Contraction ratio, 5; nozzle area, 1.60 sq in.						
324	0.144	0.426	0.570	2.96	74.5	7250
325	.140	.421	.561	3.00	77.0	7610
326	.142	.409	.551	2.88	76.0	7640
328	.142	.449	.591	3.16	82.5	7760
329	.141	.446	.607	3.30	83.5	7620
330	.141	.468	.609	3.32	83.5	7600
332	.141	.471	.612	3.34	84.0	7600
336	.142	.478	.620	3.37	81.0	7240
338	.140	.471	.611	3.36	84.0	7610
339	.147	.462	.609	3.14	83.0	7550
340	.147	.466	.613	3.17	83.0	7500
341	.147	.468	.615	3.18	83.0	7470
342	.147	.471	.618	3.20	84.0	7510
Contraction ratio, 6; nozzle area, 1.33 sq in.						
159	0.146	0.456	0.602	3.12	102	7640
160	.146	.456	.602	3.12	102.5	7670
161	.145	.458	.603	3.16	103	7720
162	.145	.461	.606	3.18	103.5	7720
163	.145	.458	.603	3.16	102.5	7690
168	.142	.451	.593	3.18	101	7690
169	.144	.453	.597	3.14	101	7640
170	.143	.456	.599	3.19	101	7610
171	.144	.458	.592	3.18	102	7760
351	.134	.419	.553	3.13	93	7800
352	.140	.442	.582	3.16	101	8050
353	.147	.449	.596	3.06	102	7940
354	.145	.446	.591	3.07	102	8000
355	.145	.459	.604	3.16	104	8000
356	.145	.459	.604	3.16	102	7840
357	.145	.464	.609	3.20	103.5	7900
359	.145	.461	.606	3.18	104	7970
360	.144	.466	.610	3.22	96	7850
361	.144	.457	.601	3.17	101	7800
362	.143	.457	.600	3.19	102	7910
363	.143	.459	.602	3.21	103	7940

TABLE II. - SUMMARY OF RESULTS

Contraction ratio	Nozzle throat area, sq in.	Chamber pressure, lb/sq in. abs		Heat-transfer rate		Characteristic exhaust velocity, c*, observed		Correction factors		Corrected c*, percent efficiency
		Theoretical	Experimental	$\frac{Btu}{sec}$	$\frac{Btu}{(sq\ in.)(sec)}$	$\frac{ft}{sec}$	Percent efficiency	Momentum pressure loss	Heat transfer	
1.5	5.33	29.3	24.9	246	1.10	7100	86.3	0.895	1.030	79.6
2	4.00	39.0	33.2	324	1.45	7310	88.9	.946	1.040	87.5
3	2.67	58.5	52.2	366	1.67	7890	95.8	.965	1.045	96.6
4	2.00	78.0	66.8	418	1.92	7720	93.7	.976	1.050	96.0
5	1.60	97.6	81.5	630	2.90	7530	91.4	.987	1.070	96.5
6	1.33	117	101.5	690	3.19	7810	94.8	.988	1.072	100.0

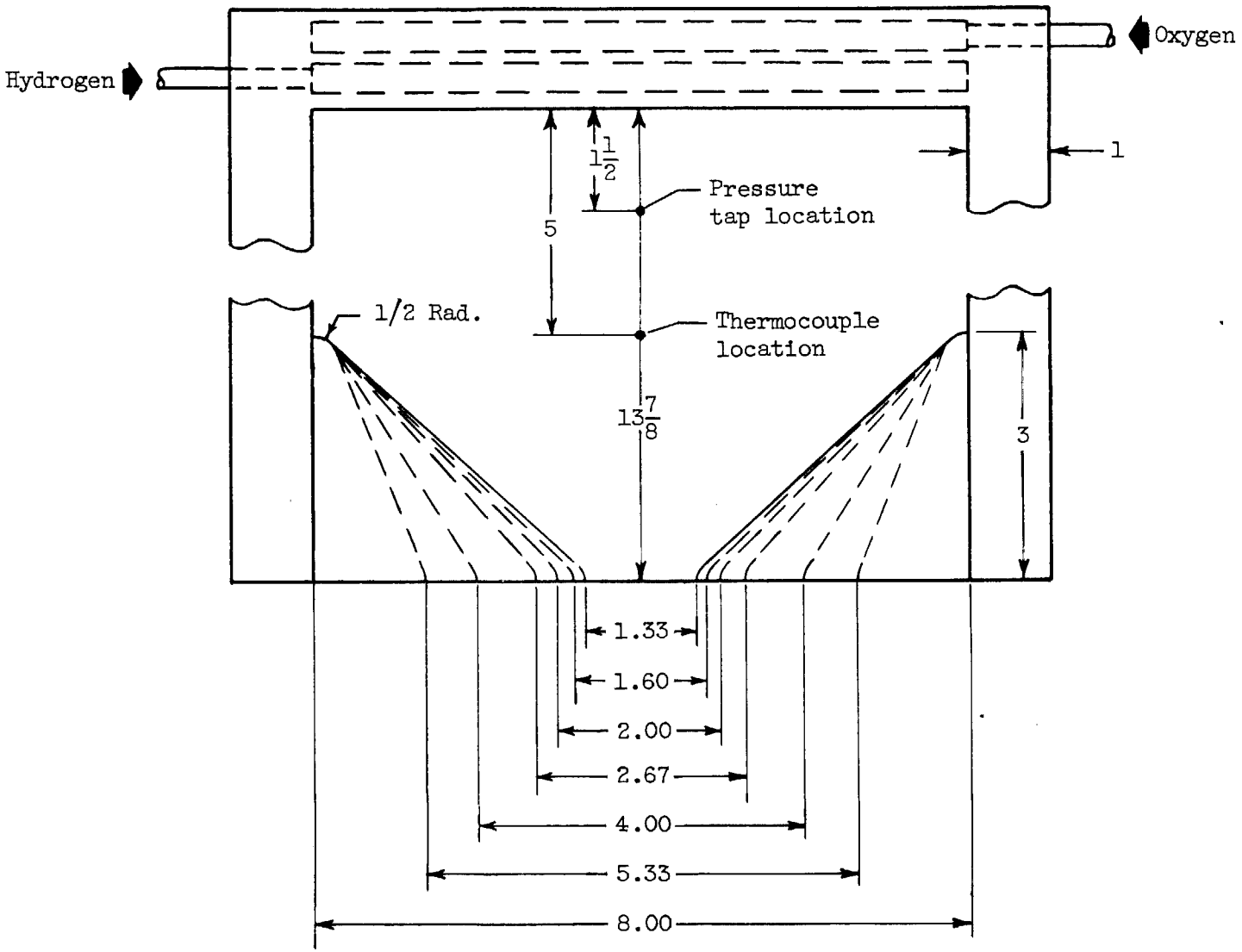

Figure 1. - Engine and nozzle configuration. (All dimensions in inches.)

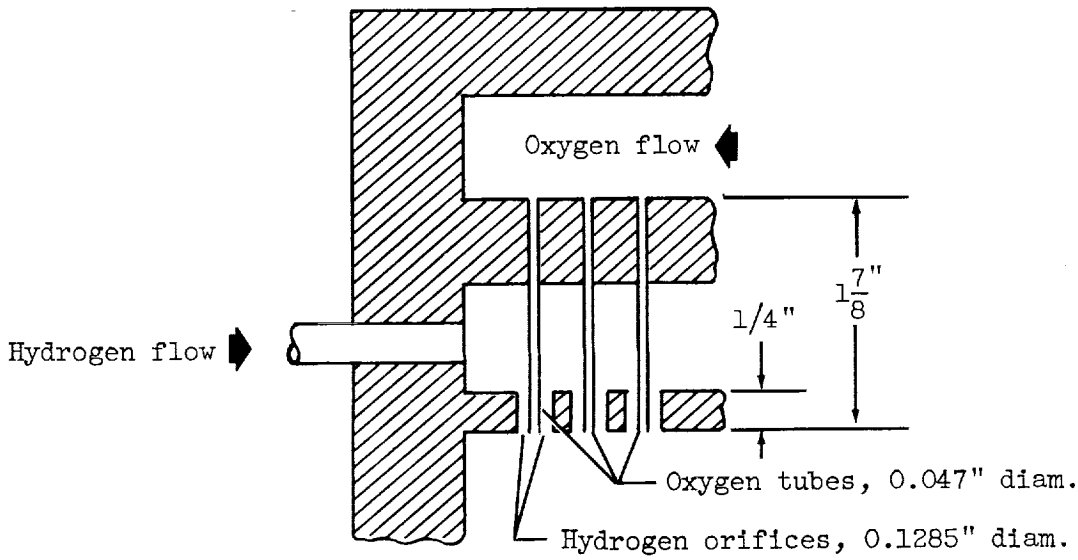

Figure 2. - Typical injector section.

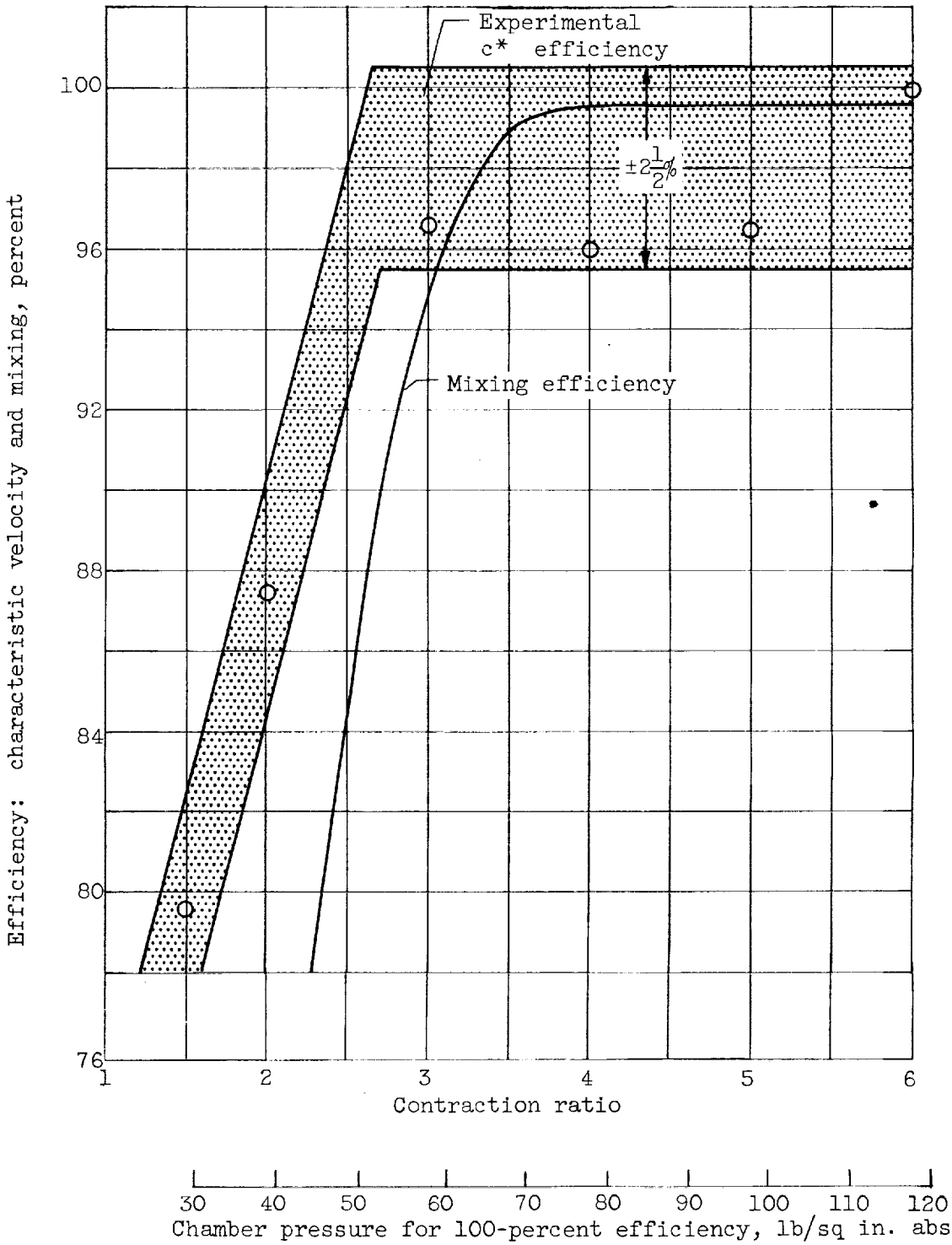

Figure 3. - Effect of contraction ratio on performance.